Novel Temporal Zone Plate Designs With Improved Energy Efficiency and Noise Performance

Bo Li, *Student Member, IEEE*, Shuqin Lou, and José Azaña, *Member, IEEE*

***Abstract*—We propose and demonstrate novel temporal zone plate designs offering a higher energy efficiency and an improved background noise performance than previously proposed approaches using similar experimental configurations. Two kinds of novel temporal zone plates, namely, temporal amplitude zone plates and temporal phase Fresnel lenses, are introduced and studied. The proposed designs are demonstrated for optical linear pulse compression. In the reported experiments, temporal amplitude zone plates are shown to provide a 96% improvement in energy efficiency (or light-collecting efficiency) and significantly reduce noise background as compared with equivalent temporal intensity zone plates. On the other hand, a temporal phase Fresnel lens is shown to offer an ideal light-collecting efficiency of 100%, greatly exceeding the efficiency of an equivalent temporal phase zone plate. Performance in a practical setup is however limited by the achievable modulation bandwidth and a 37% efficiency improvement over previous designs is experimentally demonstrated.**

***Index Terms*—Amplitude modulation, intensity modulation, optical pulse compression, optical signal processing, phase modulation.**

I. Introduction

THERE is a beautiful space-time duality between the equations that describe the paraxial diffraction in the space domain and the dispersive propagation in the time domain [1]–[19]. This duality leads to the concept of "a time lens", which is the temporal counterpart of a space lens. By suitably combining dispersion and a time lens, applications such as temporal imaging [5]–[8], linear pulse compression [9]–[11], time-to-frequency mapping [12], [13], and frequency-to-time mapping [14]–[17] of optical waveforms have been realized.

A time lens is conventionally implemented by imparting a quadratic phase shift, or linear frequency chirp, across a signal in the temporal domain. A main figure of merit of a time lens is given by its time-bandwidth product (TBP), which is the product of the temporal aperture (typically defining the maximum duration of the signal under analysis) and the frequency bandwidth (typically defining the system temporal resolution).

Manuscript received August 23, 2014; revised October 20, 2014; accepted October 22, 2014. Date of publication October 27, 2014; date of current version November 24, 2014. This work was supported by the Natural Science and Engineering Research Council of Canada and the China Scholarship Council.

B. Li is with the School of Electronic and Information Engineering, Beijing Jiaotong University, Beijing, 100044, China, and also with the Institut National de la Recherche Scientifique Energie, Matériaux et Télécommunications, Montréal, QC H5A 1K6, Canada (e-mail: liboresearch@gmail.com).

S. Lou is with the School of Electronic and Information Engineering, Beijing Jiaotong University, Beijing 100044, China (e-mail: shqlou@bjtu.edu.cn).

J. Azaña is with the Institut National de la Recherche Scientifique Energie, Matériaux et Télécommunications, Montréal, QC H5A 1K6, Canada (e-mail: azana@emt.inrs.ca).

Color versions of one or more of the figures in this paper are available online at http://ieeexplore.ieee.org

Digital Object Identifier 10.1109/JLT.2014.2365013

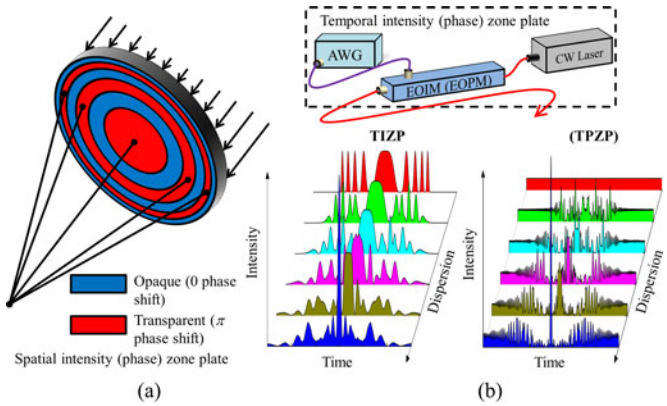

Fig. 1. Space-time duality. (a) Light focusing by a spatial intensity (phase) zone plate. (b) Pulse compression by a temporal intensity (phase) zone plate. AWG: arbitrary waveform generator; EOIM: electro-optic intensity modulator; EOPM: electro-optic phase modulator; CW Laser: continuous-wave laser.

However, in conventional time lenses, there is a severe tradeoff between the temporal aperture and temporal resolution. To solve this problem, temporal zone plates, which are the temporal counterparts of spatial zone plates, have been proposed as alternatives to time lenses [18], [19]. In previous works, two general kinds of temporal zone plates have been proposed [19]. They are based on intensity and phase modulation, respectively referred to as "temporal intensity zone plates (TIZPs)" and "temporal phase zone plates (TPZPs)". In particular, a spatial intensity zone plate is made out of a plate with alternating transmitting and opaque concentric rings with diameters being proportional to the square roots of the orders of the rings [20], whereas a spatial phase zone plate also consists of a series of concentric ring-shaped zones, which alternatively introduce 0 phase shift and π rad phase shift [21], as illustrated in Fig. 1(a). These two configurations both ensure that all the light passing through the plate, around the target wavelength, have a phase between ϕ_0 to $\phi_0 + \pi$ at the focus, where ϕ_0 is a constant phase. In this way, the light at the focus is enhanced as a result of constructive interference. As illustrated in Fig. 1(b), the time-domain analogs of spatial intensity (phase) zone plates would be temporal intensity (phase) modulation devices, which have the same amplitude-transmittance functions but as a function of the time variable (t).

Compared to time lenses, temporal zone plates do not exhibit the limiting tradeoff between the temporal aperture and temporal resolution, enabling the realization of much higher TBPs under similar experimental constraints. For example, an experimental TBP of 226, greatly exceeding the performance of a conventional linear electro-optic (EO) time lens (usually less than 5)

[11], [13], [22], has been realized using temporal zone plates based on EO modulation [19]. Therefore, the above-mentioned applications based on time lenses [1]–[19] may be improved by exploiting the significant TBP improvement offered by the temporal zone plate concept. However, similarly to their spatial counterparts, temporal zone plates are ultimately limited by their low light-collecting efficiency and the noise background of their output.

In this paper, we propose and demonstrate two novel kinds of temporal zone plates, referred to as temporal amplitude zone plates (TAZPs) and temporal phase Fresnel lenses (TPFLs). These novel designs significantly improve the performance of TIZPs and TPZPs, respectively, in terms of both light-collecting efficiency and noise background, without requiring any modification on the basic experimental configurations. In this report, we numerically and experimentally demonstrate and compare TIZPs and TAZPs for linear optical pulse compression. TIZPs and TAZPs are realized by the same electro-optic intensity modulator (EOIM) driven by different electronic waveforms, which can be generated by the same arbitrary waveform generator (AWG). Compared to TIZPs, TAZPs are demonstrated to offer higher light-collecting efficiency and lower noise background. We also numerically and experimentally demonstrate and compare TPZPs and TPFLs for linear optical pulse compression using the same electro-optic phase modulator (EOPM). The different drives of TPZPs and TPFLs are also generated by the same AWG. In the experiment, we demonstrate that TPFLs have higher light-collecting efficiency and lower noise background than their equivalent 1-st order TPZPs.

II. TAZPs

There are two types of TIZPs, which are temporal Fresnel zone plates and temporal Gabor zone plates, respectively [19]. In particular, temporal Gabor zone plates are easier to realize and more practical. Thus, we will focus on the improvement of temporal Gabor zone plates. Previously, TIZPs have been implemented by temporal intensity modulation, with a positive amplitude-transmittance function defined as follows:

$$A_G(t) = 1/2 + (1/2)\cos(at^2), \tag{1}$$

for $-\Delta t/2 < t < \Delta t/2$, in which Δt is the temporal aperture, and a/π is the modulation frequency chirp, which defines the time-lens frequency chirp. Notice that each amplitude-transmittance function is normalized in such a way that the sum of the peak magnitude of all its terms is equal to 1. (1) can be re-written as

$$A_G(t) = 1/2 + (1/4)\exp(jat^2) + (1/4)\exp(-jat^2). \tag{2}$$

Because temporal quadratic phase variations can be interpreted as being equivalent to time lenses, (2) confirms that the defined amplitude-transmittance function is equivalent to the sum of a positive and negative time lenses with the same focal time (in terms of absolute value), plus a bias term. Note that only a portion of the input light can be focused by the positive time-lens term or the negative time-lens term, while the remaining terms in (2) lead to noise background. The light-collecting efficiency of such a system, defined as the portion of light that is focused by the desired time-lens term, is given by the square of its corresponding coefficient, i.e. $(1/4)^2 \rightarrow 1/16$.

To improve the system performance in terms of light-collecting efficiency and noise background, we propose a novel TAZP, with an amplitude-transmittance function defined as

$$A_G(t) = \cos(at^2) = (1/2)\exp(jat^2) + (1/2)\exp(-jat^2), \tag{3}$$

for $-\Delta t/2 < t < \Delta t/2$, in which Δt is the temporal aperture and a/π is the modulation frequency chirp. Compared to (2), the bias term is eliminated and as a result, the associated portion of noise is canceled out. Moreover, the light-collecting efficiency of the TAZP is now given by $(1/2)^2 \rightarrow 1/4$, which is 4 times higher than that of a TIZP. In practice, the achieved improvement is limited by the finite temporal aperture of the temporal zone plate: a higher improvement ($\leq$4) is achieved as the temporal aperture is increased.

Similarly to TIZPs, the electronic waveforms can be obtained from a high-speed AWG. For a given chirp factor a, the temporal aperture must be limited due to finite bandwidth of the AWG. Based on the Nyquist-Shannon sampling theorem [23], the sampling rate f_s of the AWG should be at least two times larger than the bandwidth of the electronic waveform. Consequently, the temporal apertures of TAZPs must satisfy the following inequality $\Delta t < f_s\pi/|a|$. Notice that the total frequency bandwidth excursion produced by a quadratic phase $\phi(t) = nat^2$ along an aperture Δt is $\Delta f = |na|\Delta t/\pi$ [7], where $n = 1$ or -1. This total bandwidth excursion determines the temporal resolution of the time-lens system. In particular, for the case of a temporal imaging system with a rectangular temporal aperture function, the temporal resolution ($\delta\tau$) is given by $\delta\tau = 1/\Delta f$ [6], [7]. Hence, the temporal resolutions of TAZPs are finally determined by the following inequality $\delta\tau \geq 1/|n|\, f_s$. Thus, the temporal resolution is directly limited by the modulating signal frequency bandwidth, in turn fixed by the AWG bandwidth. In addition, further improvement on the temporal resolution may be potentially achieved by combining a temporal zone plate with a time-domain telescope scheme; this configuration may potentially enable to combine the advantages of a temporal zone plate, in terms of large temporal aperture, and a time-lens system, in terms of high temporal resolution [24].

The proposed TAZP can be practically realized by using an EOIM, e.g., a conventional EO Mach-Zehnder modulator, which is driven by a modulating electronic waveform with a temporal profile defined as the expression in (3). Recall that the optical field transfer function of the conventional EO Mach-Zehnder intensity modulator is given by [25]

$$A_{\mathrm{MZ}}(t) = \cos[\kappa V(t) + \kappa V_{\mathrm{Bias}}/2], \tag{4}$$

where $V(t)$ is the electronic drive voltage, κ is the EO coefficient, and V_{Bias} is the bias voltage. As shown by (4), the optical field transfer function can be estimated to be linearly proportional to the electronic drive voltage when $|\kappa V(t)| << \pi/2$ and $\kappa V_{\mathrm{Bias}}/2 = (-\pi/2) + 2m\pi$, i.e., $A_{\mathrm{MZ}}(t) = \sin[\kappa V(t)] \approx \kappa V(t)$, where m is an integer. We show the power transfer function of the EOIM in Fig. 2 [25], and illustrate

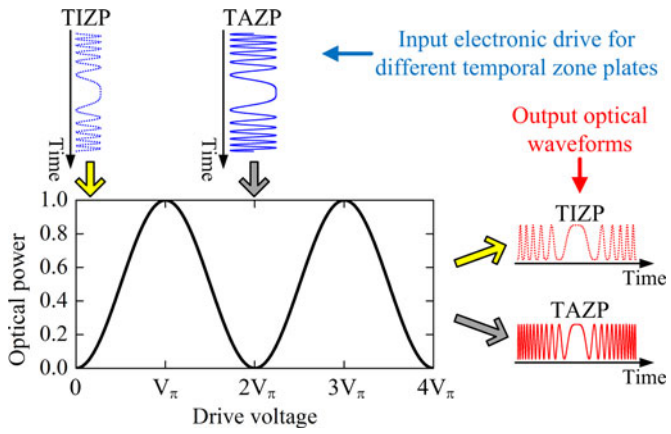

Fig. 2. Illustration of the two suggested different ways to drive the EOIM, resulting in two different temporal zone plates, i.e. TIZP and TAZP.

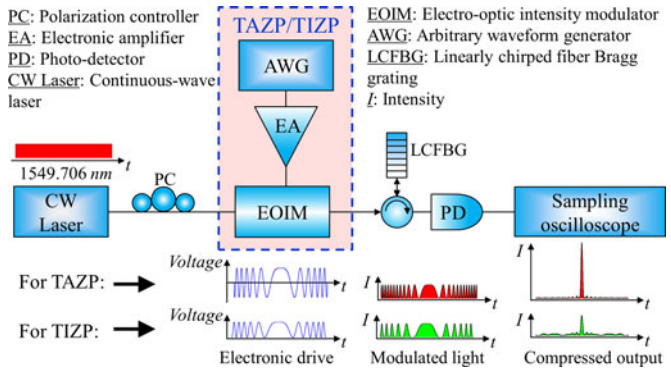

Fig. 3. Experimental scheme for linear optical pulse compression using the TAZP and the TIZP, with the terminology used in the text.

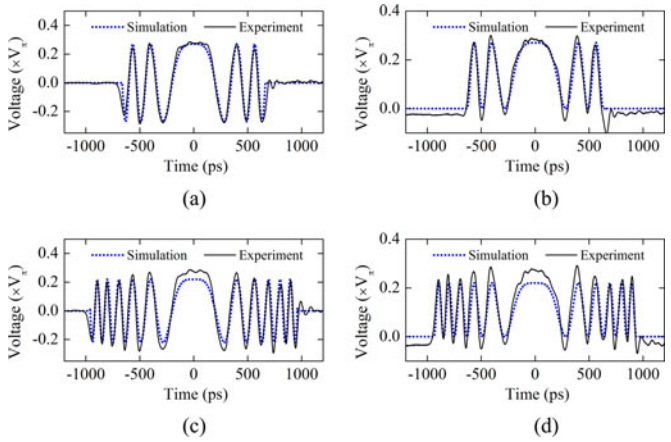

Fig. 4. The electronic drive waveforms for TAZPs (a, c) and TIZPs (b, d). We did four experiments. In particular, the temporal aperture for (a) and (b) is 1.33 ns, whereas the temporal aperture for (c) and (d) is 1.88 ns. The measured waveforms (solid black) have a good agreement with the target waveforms (dotted blue), which are calculated by (1) and (3) in the numerical simulation.

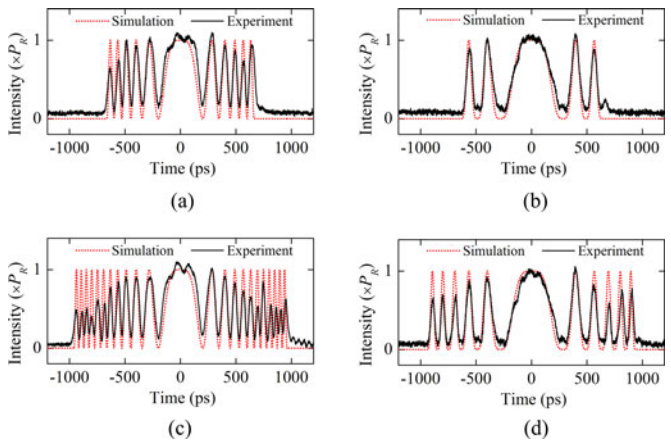

Fig. 5. Temporal intensity profiles of the optical modulated waveforms for TAZPs (a, c) and TIZPs (b, d). The temporal aperture for (a, b) and (c, d) are 1.33 ns and 1.88 ns, respectively. The Power P_R is the peak power of modulated waveforms. The measured waveforms (solid black) have a good agreement with the target waveforms (dotted red), which are calculated by the square of (1) and (3) in the numerical simulation. The slight deviation between the experimental and calculated results are due to the limited sampling rate (bandwidth) of AWG.

how to realize two different kinds of temporal zone plates (TIZPs and TZAPs) based on this same device. The electronic drive voltages for the two cases are generated according to (1) and (3), respectively, and the bias for the two cases is fixed around the same point $[(-\pi/2)+2\,m\pi]$. Note that the optical field transfer function is linear at this point, as defined above, as long as the amplitude of the electronic drive is set as a small fraction of V_π. To increase the amplitude electronic drive (so that the output waveform will have a higher peak power), the electronic waveform can be properly programmed as $V\,(t) = \arcsin\,[A_{\rm MZ}\,(t)]/\kappa$. By doing so, the nonlinearity of the optical field transfer function could be compensated for and the full swing of the modulator response could be potentially utilized. As anticipated, the driving voltage functions in (1) and (3) are directly transferred into the optical wavefields at the modulator output; this results in a positive-only optical wavefield for the TIZP design and an alternating positive and negative optical wavefield for the TAZP design, leading to the different intensity profiles for the output waveforms, as illustrated in Fig. 2. Interestingly, the proposed TAZP design has no counterpart in the spatial domain and is a totally new concept. Based on the space-time duality, a spatial amplitude zone plate design offering a higher energy efficiency than a conventional spatial intensity zone plate may be realized by spatial amplitude modulation.

To compare the performance of a TAZP and a TIZP, we set up a linear optical pulse compression experiment. To implement linear optical pulse compression, the continuous-wave light is firstly modulated with a linear frequency chirp, which is realized by a TAZP or a TIZP. Considering the quadratic phase provided by a TAZP or a TIZP, which is $\phi\,(t) = nat^2$ [see (2) and (3)], where $n = -1$ or 1, the corresponding linear frequency chirp is given by na/π. The chirped light is subsequently compensated through group-velocity dispersion, where the dispersive frequency chirp must be fixed to exactly compensate for the chirp induced by the temporal zone plate, i.e., $\ddot{\Phi}{=}{-}1/2\,na$, where $\ddot{\Phi}$ is the amount of the group-velocity dispersion [6], [8], [11]. An illustration of the conducted

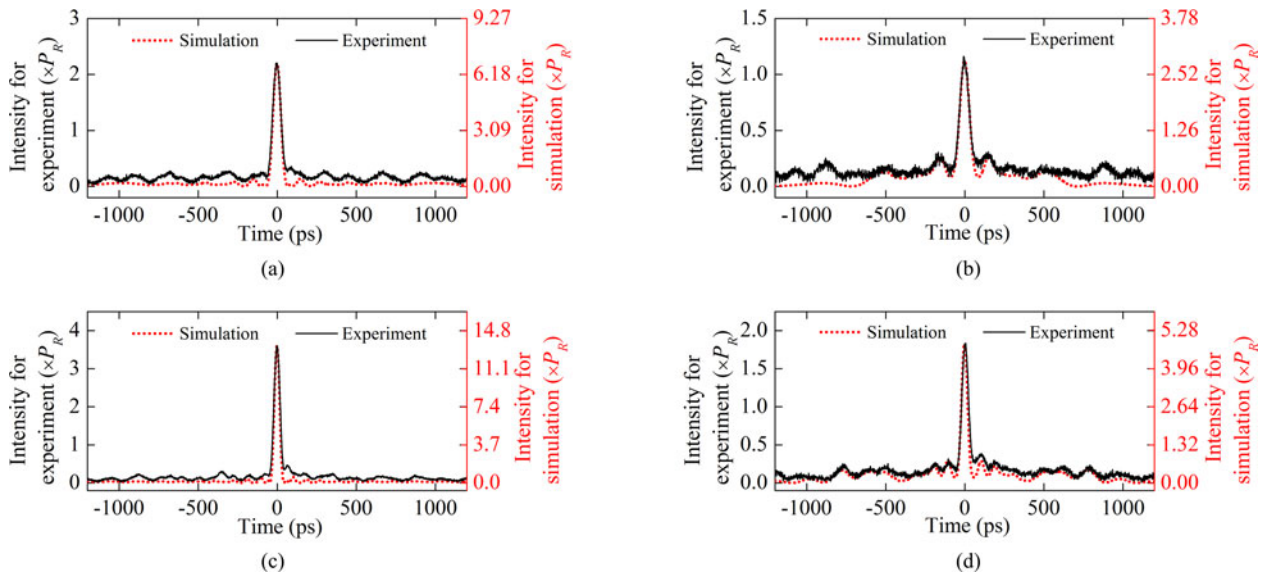

Fig. 6. The optical temporal waveforms of the system outputs for TAZPs (a, c) and TIZPs (b, d). (a)–(d) corresponds to the temporal zone plates in Fig. 5(a)–(d), respectively. Both calculated and experimental results show that a TAZP has a higher light-collecting efficiency than a TIZP.

experiment is shown in Fig. 3. Light from a continuous-wave (CW) laser at a wavelength of 1,549.706 nm is sent through a 40-GHz EOIM ($V_\pi = 3.9$ V), which is driven by the electronic waveforms generated by a 24 Gsamples/s AWG and amplified by a 12.5-GHz electronic amplifier. The laser provides the same average power for all reported experiments using a TIZP and a TAZP, respectively. The modulated light is sent through a reflective linearly chirped fiber Bragg grating (LCFBG, working from 1548.91 nm to 1552.52 nm), which introduces a predominantly 1st-order dispersion of $-10{,}000$ ps/nm. After dispersion, the light is measured with a 45-GHz photo-detector coupled to an electronic sampling oscilloscope.

Fig. 4 shows the numerically calculated (dotted blue) and measured (solid black) electronic waveforms for TAZPs (a, c) and TIZPs (b, d). To fully compare the performance of these two different temporal zone plates, we did four experiments. In particular, the temporal aperture for Fig. 4(a) and (b) is 1.33 ns, whereas the temporal aperture for Fig. 4(c) and (d) is 1.88 ns. There is a better agreement between numerical simulation and experiment for Fig. 4(a) and (b), for which the reason is that Fig. 4(c) and (d) requires a larger modulating bandwidth to implement the target waveform.

Fig. 5 demonstrates the corresponding numerically calculated (dotted red) and measured (solid black) optical modulated waveforms for TAZPs (a, c) and TIZPs (b, d). The temporal aperture for Fig. 5(a, b) and (c, d) are 1.33 ns and 1.88 ns, respectively. The Power P_R is the peak power of modulated waveforms. The slight deviation between the experimental and calculated results is due to the limited sampling rate of AWG. Similar to Fig. 4, the deviation for Fig. 5(c, d) is more significant than that for Fig. 5(a, b).

Fig. 6 shows the corresponding numerically calculated (dotted red) and measured (solid black) output optical waveforms for linear pulse compression based on TAZPs (a, c) and TIZPs (b, d). There is a good agreement between numerical simulation and experiment in terms of intensity profile. The numerically calculated peak powers for the waveforms in (a)–(d) are $6.817\,P_R$, $2.838\,P_R$, $13.334\,P_R$, and $4.833\,P_R$, respectively. Therefore, the energy efficiencies for (a) and (c) are 2.4 and 2.76 times higher than those for (b) and (d), respectively. As anticipated, the improvement factor is lower than 4 due to the practical finite temporal aperture. As shown in Fig. 5, the modulation profiles for the TIZP and the TAZP are similar in the center area (around $t = 0$) and different in the other area ($t >> 0$ and $t << 0$). And thus, the improvement is mainly contributed by the area on the two sides ($t >> 0$ and $t << 0$). Therefore, the improvement factor increases as the temporal aperture. In the experiment, the measured peak powers for the waveforms in (a)–(d) are $2.203\,P_R$, $1.124\,P_R$, $3.599\,P_R$, and $1.835\,P_R$, respectively, which are smaller than the numerically calculated values. The first reason for the lower experimental peak powers is that the LCFBG has an insertion loss of 2.77 dB. The second reason is due to the deviation between the experimental and calculated waveforms shown in Fig. 5. Nevertheless, the energy efficiencies for (a) and (c) are 1.96 and 1.9613 times higher than those for (b) and (d), in line with our predictions on the improved performance offered by a TAZP as compared with a TIZP. The deviation between the measured improvement factors and the calculated values is mainly due to the distortion of the experimental modulating waveforms as compared with the calculated ones shown in Fig. 5; thus, the second measured improvement factor (1.9613) exhibits a more pronounced deviation from the calculated value (2.76). In addition, as shown by both numerical simulation and experimental results in Fig. 6, the noise backgrounds in (a) and (c) are lower than those in (b) and (d), proving the anticipated improvement offered by a TAZP versus a conventional TIZP, as predicted by (1)–(3). In addition, the experimentally measured resolutions (estimated as intensity FWHM) for (a)–(d) are 60.82 ps, 73.26 ps, 44.82 ps, and 50.55 ps, respectively, in good agreement with the

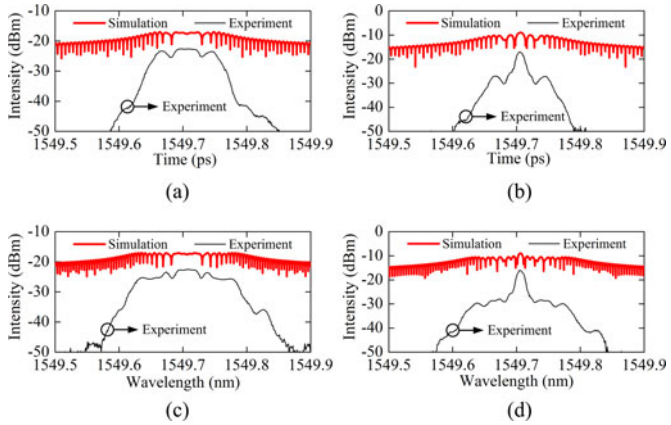

Fig. 7. The spectra of the optical pulse waveforms at the system output for TAZPs (a, c) and TIZPs (b, d). (a)-(d) corresponds to the temporal zone plates in Fig. 5(a)–(d), respectively. As predicted by (1)–(3), there is a bias term in TIZP, which corresponds to the center lobes in (b) and (d). However, for TAZP, there is no bias term, as proved by the nearly flat spectra in (a) and (c).

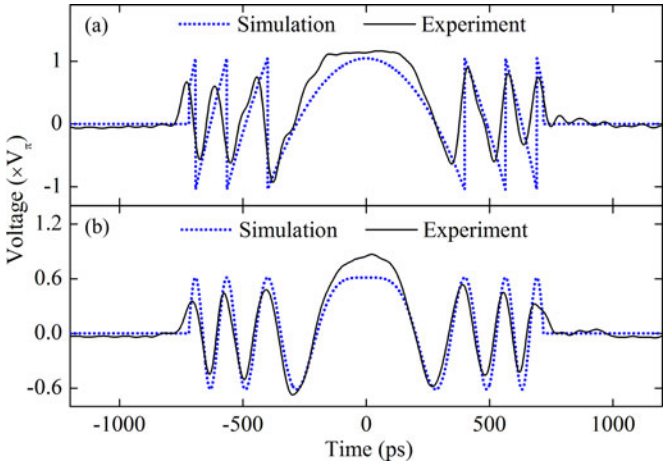

Fig. 8. Electronic modulation waveforms for a TPFL (a) and a 1st-order TPZP (b).

calculated values, i.e., 57.06 ps, 72.71 ps, 38.58 ps, and 45.08 ps, respectively. Both experimental and calculated results show that a TAZP has a slightly better resolution than a TIZP, which is mainly due to the improved energy efficiency and lower noise background.

Fig. 7 presents the corresponding numerically calculated (dotted red) and measured (solid black) output optical spectra for linear pulse compression systems based on TAZPs (a, c) and TIZPs (b, d). There is an excellent agreement between numerical simulations and experiments. As predicted by (1)–(3), there is a bias term in TIZPs, which corresponds to the center spectral lobes in (b) and (d), while for TAZPs there is no bias term, as proved by the nearly flat spectra in (a) and (c). In addition, the bandwidths of the output spectra are inversely proportional to the temporal resolution of these systems.

III. Temporal Phase Fresnel Lens

Although TPZPs have higher energy efficiency than TIZPs, this is still limited to ~40% [19]. In the spatial domain, there is a special phase zone plate with "distorted profile" – phase Fresnel lens [26]–[28], which can ideally provide an energy efficiency of 100%. In the space domain, an ideal lens is equivalent to quadratic phase modulation, i.e., $\phi(x) = \gamma x^2$, where γ is a constant. To realize a large phase modulation amplitude, the lens should be fabricated with a large thickness, which is difficult to realize in practice. However, by utilizing the periodical property of sinusoidal function, the phase modulation profile can be represented as $\phi(x) = \gamma x^2 - 2k\pi$, when $2k\pi < \gamma x^2 < (2k+1)\pi$ and thus, the thickness of the lens is greatly compressed whereas the energy efficiency of the phase Fresnel lens is 100% [26]–[28]. In the temporal domain, the temporal counterpart of a spatial phase Fresnel lens, namely "temporal phase Fresnel lens", can be realized through temporal phase modulation with a profile defined by the following equation,

$$\phi(t) = at^2 - 2k\pi, \text{ when } 2k\pi < at^2 < (2k+1)\pi, \quad (5)$$

where k is an integer. The concept of the TPFL has been proposed in the previous work [29]. However, we experimentally demonstrate and compare TPFLs and TPZPs for linear pulse compression for the first time.

In practice, a TPFL can be realized by using an EOPM driven by electronic waveforms generated by an AWG, using a similar configuration to a TPZP [19]. A TPZP is a type of temporal zone plate and can be realized by phase modulation with a sinusoidal modulation profile:

$$\phi_{GP}(t) = \Gamma_0 \cos(at^2), \quad (6)$$

for $-\Delta t/2 < t < \Delta t/2$, in which Δt is the temporal aperture, a/π is the modulation frequency chirp, and Γ_0 is the phase-modulation amplitude. Similar to (2) and (3), the phase modulation profile of a TPZP can be represented to be equivalent to a set of positive and negative time lenses (or quadratic phase terms) at different focal times, i.e., each with a different frequency chirp, depending on the integer order n [19]:

$$H_{GP}(t) = \exp[j\phi_{\mathrm{GP}}(t)] = \sum_{n=-\infty}^{\infty} j^n J_n(\Gamma_0) \exp(jnat^2), \quad (7)$$

where n is the order and $J_n(.)$ is the n-th order Bessel function.

Similar to a TIZP, a TPZP can provide a linear frequency chirp of na/π, as shown by (7), whereas a TPFL can provide a linear frequency chirp of a/π, as shown by (5). By using dispersion subsequently, which is fixed to compensate the frequency chirp, i.e., $\ddot{\Phi}=-1/2na$ for the TPZP and $\ddot{\Phi}=-1/2a$ for the TPFL, linear pulse compression can be implemented. Since a TPFL doesn't have high order, we will focus on the comparison of a TPFL and a 1st-order TPZP. Compared to a 1st-order TPZP, which has an energy efficiency of 33.5%, the TPFL has a different phase modulation profile, and it can ideally focus all (100%) of the input light at its focal point along the time domain. However, a TPFL needs a faster AWG than a TPZP, because its profile varies faster, as shown in Fig. 8. For example, by the use of a 24 Gsamples/s AWG, the electronic drive for a TPFL and a TPZP are shown in Fig. 8. Note that the experimental scheme for linear optical pulse compression based on a TPFL or a TPZP

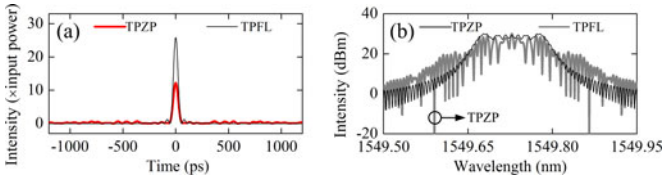

Fig. 9. The temporal intensity profiles (a) and the spectra (b) of the compressed output pulses for a TPFL and a TPZP, as obtained in numerical simulation.

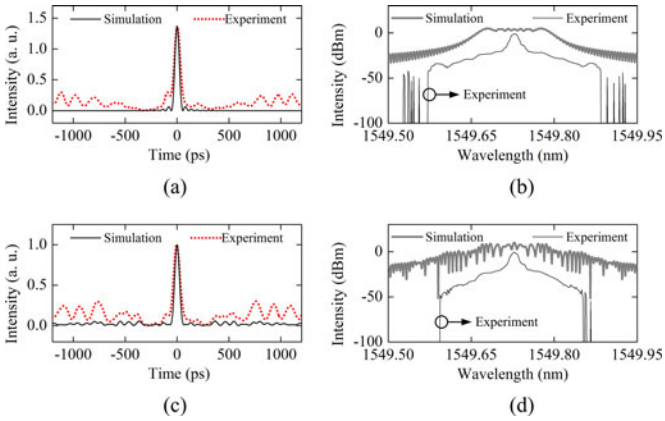

Fig. 10. The simulated and measured temporal intensity profiles (a, c) and spectra (b, d) of the compressed output pulses for a TPFL (a, b) and a TPZP (c, d). The results of simulation (thick grey lines) in (b, d) are shifted to avoid overlapping the experimental results (thin black).

is similar to the one based on temporal intensity/amplitude zone plates, Fig. 2, except that the EOIM is replaced by an EOPM. The measured electronic waveform obtained in the experiment for the TPFL has a larger deviation from the calculated curve obtained in the simulation than for the case of a TPZP. Additionally, the phase modulation amplitudes for a TPFL and a TPZP are π rad and 1.84 rad [19], respectively.

At first we compared the compressed outputs for the TPFL and the TPZP in the numerical simulation, as shown in Fig. 9. Note that the CW light beyond the temporal aperture is not considered in the numerical simulation. The peak powers of the TPFL output (thin black line) and the TPZP output (thick red line) are 25.84 and 12.25 times higher than the input CW power, respectively. In particular, the compressed output for the TPFL has a larger peak power [Fig. 9(a)], because a TPFL has a significantly higher light-collecting efficiency, ideally approaching 100%. The pulse widths for the TPFL and TPZP are similar, since the frequency bandwidths induced by the two zone plates are identical. Moreover, the output spectrum of the TPFL [thin black line in Fig. 9(b)] is flatter than that of the TPZP [thick grey line in Fig. 9(b)], an indication of the fact that the TPFL output pulse has a reduced noise background along the time domain. The corresponding measured compressed output pulses are shown in Fig. 10. It is important to note that the CW light beyond the temporal aperture is not filtered in the experiment so that there is significant noise beyond the temporal aperture window [Fig. 10(a, c)], which in turn translates into the presence of a central lobe in each of the corresponding spectra [Fig. 10(b, d)]. Except for these noise patterns, there is an excellent agreement between the numerical simulation (dotted red lines) and the experiment (solid black lines). In our experiment, the output pulse for TPFL [Fig. 10(a)] has a 1.37 times larger peak power and a lower noise background (within the temporal aperture) than that obtained using the TPZP [Fig. 10(c)]. As predicted above, the peak-power improvement factor is smaller than the theoretical value of 2.1 (25.84/12.25), which is a result of the deviation between measured and calculated modulation waveforms in Fig. 8. Finally, the measured TPFL output also exhibits the expected flatter spectrum as compared with the TPZP output, as shown in Fig. 10(b) and (d).

As discussed above, a TPFL provides higher energy efficiency and lower noise than a TPZP. However, these improvements are at the cost of using an electronic drive with a higher bandwidth, where the sharp changes in the electronic drive are difficult to realize, as shown in Fig. 8. Thus, for a given modulating bandwidth, the temporal aperture of a TPFL is smaller than that of a TPZP. As a result, a TPFL is preferable in applications where the noise tolerance is very low.

IV. Conclusion

In summary, two different kinds of novel temporal zone plates have been introduced and investigated, respectively based on temporal amplitude modulation and temporal phase modulation. These novel temporal zone plates effectively improve the light-collecting efficiency and noise background performance of previous temporal zone plate designs, while using identical experimental setups. Compared with previous TIZPs, TAZPs provide a 96% improvement in energy efficiency and significantly reduce noise background. Compared with previous TPZPs, TPFLs provide a 37% improvement in energy efficiency and reduce noise background. The proposed temporal zone plates should prove particularly interesting for linear optical pulse generation and compression experiments and related applications.

References

[1] B. H. Kolner and M. Nazarathy, "Temporal imaging with a time lens," *Opt. Lett.*, vol. 14, pp. 630–632, Jun. 1989.
[2] B. H. Kolner, "The pinhole time camera," *J. Opt. Soc. Amer. A*, vol. 14, pp. 3349–3357, Dec. 1997.
[3] E. Treacy, "Optical pulse compression with diffraction gratings," *IEEE J. Quantum Electron.*, vol. 5, no. 9, pp. 454–458, Sep. 1969.
[4] C. V. Bennett and B. Kolner, "Principles of parametric temporal imaging. I. System configurations," *IEEE J. Quantum Electron.*, vol. 36, no. 4, pp. 430–437, Apr. 2000.
[5] C. V. Bennett, R. P. Scott, and B. H. Kolner, "Temporal magnification and reversal of 100 Gb/s optical data with an up-conversion time microscope," *Appl. Phys. Lett.*, vol. 65, pp. 2513–2515, Nov. 1994.
[6] B. H. Kolner, "Space-time duality and the theory of temporal imaging," *IEEE J. Quantum Electron.*, vol. 30, no. 8, pp. 1951–1936, Aug. 1994.
[7] B. H. Kolner, "Generalization of the concepts of focal length and f-number to space and time," *J. Opt. Soc. Amer. A*, vol. 11, pp. 3229–3234, Dec. 1994.
[8] R. Salem, M. A. Foster, A. C. Turner, D. F. Geraghty, M. Lipson, and A. L. Gaeta, "Optical time lens based on four-wave mixing on a silicon chip," *Opt. Lett.*, vol. 33, pp. 1047–1049, May 2008.
[9] J. Bjorkholm, E. Turner, and D. Pearson, "Conversion of CW light into a train of subnanosecond pulses using frequency modulation and the dispersion of a near-resonant atomic vapor," *Appl. Phys. Lett.*, vol. 26, pp. 564–566, May 1975.
[10] J. Wigmore and D. Grischkowsky, "Temporal compression of light," *IEEE J. Quantum Electron.*, vol. 14, no. 4, pp. 310–315, Apr. 1978.

[11] J. van Howe, J. Hansryd, and C. Xu, "Multiwavelength pulse generator using time-lens compression," *Opt. Lett.*, vol. 29, pp. 1470–1472, Jul. 2004.
[12] M. Kauffman, W. Banyai, A. Godil, and D. Bloom, "Time-to-frequency converter for measuring picosecond optical pulses," *Appl. Phys. Lett.*, vol. 64, pp. 270–272, Jan. 1994.
[13] M. A. Foster, R. Salem, D. F. Geraghty, A. C. Turner-Foster, M. Lipson, and A. L. Gaeta, "Silicon-chip-based ultrafast optical oscilloscope," *Nature*, vol. 456, pp. 81–84, Nov. 2008.
[14] R. Llorente, R. Clavero, and J. Marti, "Performance analysis of polarimetric PMD monitoring by real-time optical Fourier transformers," *IEEE Photon. Technol. Lett.*, vol. 18, no. 12, pp. 1383–1385, Jun. 2006.
[15] R. P. Scott, N. K. Fontaine, D. J. Geisler, and S. Yoo, "Frequency-to-time-assisted interferometry for full-field optical waveform measurements with picosecond resolution and microsecond record lengths," *IEEE Photon. J.*, vol. 4, no. 3, pp. 748–758, Jun. 2012.
[16] T. T. Ng, F. Parmigiani, M. Ibsen, Z. Zhang, P. Petropoulos, and D. J. Richardson, "Compensation of linear distortions by using XPM with parabolic pulses as a time lens," *IEEE Photon. Technol. Lett.*, vol. 20, no. 13, pp. 1097–1099, Jul. 2008.
[17] M. A. Muriel, J. Azaña, and A. Carballar, "Real-time Fourier transformer based on fiber gratings," *Opt. Lett.*, vol. 24, pp. 1–3, Jan. 1999.
[18] M. T. Flores-Arias, L. Chantada, C. Bao, M. V. Pérez, and C. Gómez-Reino, "Temporal zone plate," *J. Opt. Soc. Amer. A*, vol. 25, pp. 3077–3082, Dec. 2008.
[19] B. Li, M. Li, S. Lou, and J. Azana, "Linear optical pulse compression based on temporal zone plates," *Opt. Exp.*, vol. 21, pp. 16814–16830, Jul. 2013.
[20] R. W. Wood, *Zone-Plate*. New York, NY, USA: Macmillan, 1934.
[21] L. Rayleigh, *Wave Theory of Light*, Edinburgh, Scotland: A & C Black, 1888.
[22] L. E. Munioz-Camuniez, V. Torres-Company, J. Lancis, J. Ojeda-Castaneda, and P. Andres, "Electro-optic time lens with an extended time aperture," *J. Opt. Soc. Amer. B*, vol. 27, pp. 2110–2115, Oct. 2010.
[23] C. E. Shannon, "Communication in the presence of noise," *Proc. IEEE*, vol. 86, no. 2, pp. 447–457, Feb. 1998.
[24] M. A. Foster, R. Salem, Y. Okawachi, A. C. Turner-Foster, M. Lipson, and A. L. Gaeta, "Ultrafast waveform compression using a time-domain telescope," *Nature Photon.*, vol. 3, pp. 581–585, Sep. 2009.
[25] P. J. Winzer and R.-J. Essiambre, "Advanced optical modulation formats," *Proc. IEEE*, vol. 94, no. 5, pp. 952–985, May 2006.
[26] K. Miyamoto, "The phase Fresnel lens," *J. Opt. Soc. Amer.*, vol. 51, pp. 17–20, Jan. 1961.
[27] M. H. Horman, "Efficiencies of zone plates and phase zone plates," *Appl. Opt.*, vol. 6, pp. 2011–2013, Nov. 1967.
[28] J. Kirz, "Phase zone plates for X-rays and the extreme UV," *J. Opt. Soc. Amer.*, vol. 64, pp. 301–309, Mar. 1974.
[29] D. Yang and S. Kumar, "Realization of optical OFDM using time lenses and its comparison with optical OFDM using FFT," *Opt. Exp.*, vol. 17, pp. 17214–17226, Sep. 2009.

Bo Li (S'14) was born in Shandong, China, on November 29, 1989. He received the B.S. degree in applied physics from Shandong University, Jinan, China, in 2009, and the M.S. degree in optical communication from Beijing Jiaotong University, Beijing, China, in 2011. He started working toward the Ph.D. degree at the same university in 2011, majoring in communication and information system. Under an exchange program (from 2012 to 2014), he is currently working in the Ultrafast Optical Processing Group, Institut National de la Recherche Scientifique–Energie, Matériaux et Télécommunications–Université du Québec, Montréal, QC, Canada, under the supervision of Professor J. Azaña.

His recent research interests include ultrafast optical signal processing using space-time duality, linear pulse compression based on temporal zone plates, and incoherent-light temporal imaging of radio-frequency signals.

Shuqin Lou was born in China in 1965.

She is currently a Professor at the School of Electronic and Information Engineering, Beijing Jiaotong University, Beijing, China. Her current research interests include optical communication, optical signal process, special fiber, and fiber device.

José Azaña (M'03) received the Telecommunication Engineer degree and the Ph.D. degree in telecommunication engineering from the Universidad Politécnica de Madrid, Madrid, Spain. He is currently a Professor and Canada Research Chair at the Institut National de la Recherche Scientifique–Centre Energie, Matériaux et Télécommunications, Montreal, QC, Canada. His research interests include ultrafast photonics, optical signal processing, all-fiber and integrated-waveguide technologies, high-speed telecommunications, all-optical computing, measurement of ultrafast events, light pulse interferometry, and broadband microwave signal generation and manipulation. He has to his credit nearly 400 publications in top scientific journals and technical conferences, including more than 160 contributions in high-impact peer-review journals, and many invited and coinvited journal publications and presentations in leading international meetings.

His research studies have been recognized with several prestigious awards and distinctions at institutional, national, and international levels, including the 2008 IEEE-Photonics Society Young Investigator Award, and the 2009 IEEE-MTT Society Microwave Prize.